IIETA International Information and Engineering Technology Association
Advancing the World of Information and Engineering

Mathematical Modelling of Engineering Problems
Vol. 13, No. 1, February, 2026, pp. 16-24
Journal homepage: http://iieta.org/journals/mmep

Stagnation Point Flow of Radiative Casson Nanofluid Flow Over a Vertical Stretching Surface with Velocity Slip Effects: A Numerical Analysis

Khuram Rafique[1], Tatheer Fatima[2], Gamal Elkahlout[3*]

[1] Centre of Excellence for Social Innovation and Sustainability, Institute of Engineering Mathematics, University Malaysia Perlis, Arau 02600, Malaysia
[2] Department of Mathematics, University of Sialkot, Sialkot 51310, Pakistan
[3] School of Business Studies, Arab Open University, Riyadh 11681, Saudi Arabia

Corresponding Author Email: g.elkahlout@arabou.edu.sa

https://doi.org/10.18280/mmep.130102

Received: 8 September 2025
Revised: 6 December 2025
Accepted: 15 December 2025
Available online: 28 February 2026

Keywords:
magnetohydrodynamic, stagnation point flow, Casson nanofluid, Soret and Dufour effects, Buongiorno model, Keller–Box method, velocity slip

ABSTRACT

In the current research, the magnetohydrodynamic stagnation-point flow of a Casson nanofluid through a vertical linearly extending sheet under the effects of Soret and Dufour is explored. The Buongiorno model is used to examine Brownian motion and thermophoresis. Additionally, the velocity slip effect is also considered. Partial differential equations are transformed into ordinary differential equations using similarity variables, which are then mathematically solved through the Keller–Box technique. The graphs illustrate how various variables affect the temperature, concentration, and velocity distributions in the boundary layer. Furthermore, the results show that the concentration profile and boundary layer thickness decrease as the Soret effect parameter increases. Moreover, the temperature profile increases as the thermophoresis factor increases.

1. INTRODUCTION

The study of non-Newtonian fluids on stretching and shrinking surfaces has garnered significant attention due to their key properties in various technological and industrial fields. These include petroleum drilling, printing, polymer technology, food processing, and damping and braking systems. Many types of non-Newtonian fluids exist, including paints, quicksand, molten polymers, liquid crystals, ketchup, yoghurt, butter, and honey, as well as biological fluids like blood.

Unlike Newtonian fluids, non-Newtonian fluids do not have a predictable relationship between local shear stresses and shear rates. This results in their viscosity changing with the shear rate or its history. Consequently, no single equation can describe all the rheological properties of non-Newtonian fluids, and no one model can fully capture these features.

Consequently, researchers have developed various models to study these fluids. The effective contrast between non-Newtonian and Newtonian fluids in a system with slip and non-slip conditions was investigated by Tauviqirrahman et al. [1]. Computational modeling of the viscous characteristics of non-Newtonian fluids, as proposed by Ionescu et al. [2], involves testing. The unsteady Casson nanofluid (CNF) flow caused by buoyancy was examined by Ullah et al. [3]. The Casson fluid flow behaviour over an exponentially extending surface at the wall temperature was studied by Lee and Nadeem [4]. Several solutions for non-Newtonian CNF flow across a moving extending surface with the impact of radiation and thermal conduction were investigated by Elgazery and Elelamy [5].

Magnetohydrodynamics (MHD) flow of a non-Newtonian CNF through an extending plate is described by Lone et al. [6]. The impacts of MHD, mass, and heat transfer in the flow of a non-Newtonian Casson fluid over an oscillatory porous surface were studied by Prameela et al. [7].

In fluid mechanics, the point where the local velocity approaches zero is known as the stagnation point. Stagnation points usually occur on the surface of an object within the flow area, where the fluid velocity drops to zero due to the presence of the object. The highest mass deposition, heat transfer rate, and fluid pressure occur in the stagnation zones. The importance of analyzing stagnation-point flow in various hydrodynamic processes and manufacturing applications has attracted the attention of many scholars over the past few decades. Ali et al. [8] investigated the effects of heat radiation and a magnetic field on mixed convection stagnation point flow over a vertical extended surface. To perform a mathematical calculation, Khan et al. [9] studied stagnation-point flow of micropolar nanofluids affected by suction/injection, buoyancy, and thermophoresis. The effect of solar radiation on 2D stagnation-point nanofluid flow over an elastic plate was studied by Ghasemi and Hatami [10]. The stagnation point flow of a ferrofluid with Newtonian thermal expansion was investigated by Yasin et al. [11]. The stagnation-point flow over a linearly expanding sheet and the heat transfer process with nanofluid were studied by Alhamaly et al. [12]. The CNF flow near the stagnation point on an elastic sheet under the impact of radiation and heat generation was studied by Alrehili [13].

Research on nanofluids has been highly effective across a range of scientific and industrial fields. According to Choi and Eastman [14], a nanofluid is a synthesized suspension of colloidal nanoparticles distributed in a base liquid. Nanoparticles are particles having a size smaller than a nanometer. The nanoparticles used in nanofluids typically consist of metals or metal oxides, such as aluminum, copper, aluminum oxide, zinc oxide, Fe_2O_3, TiO_2, graphite, or carbon nanotubes. The key points of nanofluid technology are to expand the heat transfer process by enhancing the basic fluid's thermal conductivity and convective heat transfer capacity with the dispersion of nanoparticles.

Moreover, due to their small size, the nanoparticles may remain in the liquid phase for an extended period, ranging from months to years, without sedimenting. Buongiorno [15] developed a new nanofluid model that accounts for the effects of Brownian motion and thermophoresis on nanoparticle motion within a fluid dispersion. The magnetic force on a couple stress nanofluid due to a moving extended sheet with heat conduction has been discussed by Aljaloud et al. [16]. The 2D MHD flow of an expanded viscous nanofluid over a curved plate is examined by Hosseinzadeh et al. [17]. The effects of heat radiation and chemical reactions on convection and conduction in the nanofluid boundary layer caused by a porous stretching sheet have been investigated by Sedki [18]. For more detailed literature on nanoliquid flow [19-21].

MHD has a broad range of applications across multiple fields. In astrophysics, understanding phenomena such as solar winds, the behavior of interstellar plasma, and star formation is essential. In geophysics, MHD principles help explain the generation and dynamics of Earth's magnetic field caused by the movement of conducting materials in the core. In engineering, MHD is used in the design of MHD generators, which convert kinetic and thermal energy into electrical power. It is also employed in advanced cooling systems for nuclear reactors, where liquid metals act as coolants.

A Casson fluid with varying thickness flows through a stretching surface under a magnetic field, as demonstrated by Hussain et al. [22]. The effects of heat radiation and velocity slip on the stagnation-point flow of an MHD Casson fluid over an elastic surface were examined by Raza [23]. A numerical model incorporating a CNF has been proposed by Narender et al. [24] to investigate the effects of heat generation and absorption, as well as a magnetic field, on MHD stagnation-point flow over an extending plate. MHD flows at the stagnation point via a heated extended paper, including the effects of chemical reaction, Soret, and Dufour, were studied by Verma et al. [25].

In view of the above-cited literature, this study numerically investigated Casson nanoliquid flow towards a vertical flexible surface. In addition, magnetic factors, the Casson factor, porosity, thermal radiation factor, chemical reaction, and Soret and Dufour effects are considered in this research. Additionally, to address nanoparticle dispersion in the Casson fluid, the effects of Brownian motion and thermophoresis will be considered. For numerical results, the Keller–Box method is employed. There is no study in the literature on Casson nanoliquid flow over a vertical surface that incorporates velocity slip, thermal radiation, chemical reaction, Soret, and Dufour effects. To fill this gap, this research article was prepared. Further, this research has many industrial and engineering applications, including printing, food processing, polymer technology, petroleum drilling, and damping and braking systems.

This study helps answer the following questions:

- How do involved factors affect the temperature, concentration, and velocity profile of the non-Newtonian CNF?
- How do the Brownian motion thermophoresis parameters affect energy and mass transfer properties?
- How are the energy and mass transfer phenomena of CNF examined via the Keller–Box method?

2. PROBLEM FORMULATION

We study the steady 2D flow of an incompressible MHD CNF over a porous medium, focusing on a stagnation point and a linearly vertically expanding surface. The stretching/shrinking sheet is assumed to have a linear velocity in the form of $u_w(x) = ax$ ambient fluid's velocity is $u_\infty(x) = bx$, where, $a,\ b$ are constants. We suppose that the fluid is electrically conductive and exposed to a magnetic field B_0 directed perpendicular to the stretching surface. Furthermore, it is suggested that T_∞ expresses the temperature of the free stream and T_M signifies the melting temperature, where, $T_\infty > T_M$. The proportion of nanoparticles at the surface is C_w, although the proportion of ambient nanoparticles is C_∞. The geometry of the flow problem is illustrated in Figure 1.

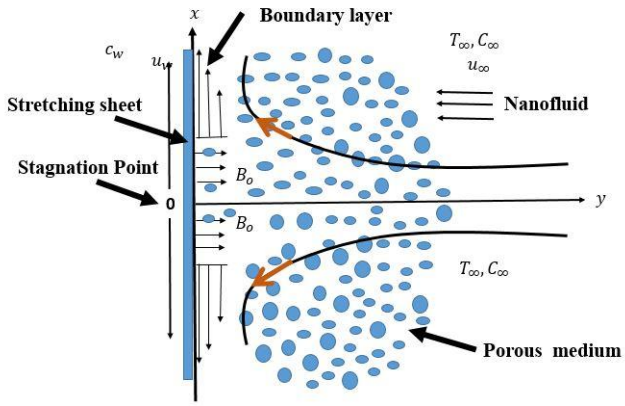

Figure 1. Flow structure of the coordinate system

Assuming that the Casson fluid rheological equation is derived by Duguma et al. [26] and Mustafa et al. [27] as given in Eq. (1):

$$\tau_{ij} = \begin{cases} 2\left(\mu_B + \dfrac{P_y}{\sqrt{2\pi}}\right)\epsilon_{ij} & \text{if } \pi > \pi_c \\ 2\left(\mu_B + \dfrac{P_y}{\sqrt{2\pi_c}}\right)\epsilon_{ij} & \text{if } \pi < \pi_c \end{cases} \tag{1}$$

In this framework, τ_{ij} signifies the stress tensor elements, μ_B specifies the plastic dynamic viscosity of the non-Newtonian, $P_y \equiv \mu_B(\sqrt{2\pi_c}/\beta)$ facts to the fluid elastic stress. Here, β is noticeable as the Casson fluid factor, π is obtained by multiplying all of the distortion rate's parts together as $\pi = \epsilon_{ij}, \epsilon_{ij}, \epsilon_{ij}$ is the $(i, j) -$ the component of the strain rate tensor and π_c denotes a threshold value of π based on the non-Newtonian methodology. For the Casson fluid flow presence examined, where, $\pi > \pi_c$, μ_f is equivalent to $\mu_B + \frac{P_y}{\sqrt{2\pi}}$, thus

yielding the kinematic viscosity as $\nu_f = \frac{\mu_B}{\rho_f}\left(1+\frac{1}{\beta}\right)$. The flow equations for the current problem are given by Kumar and Varma [28], Zulkifli et al. [29], and Hayat et al. [30].

$$\frac{\partial u}{\partial x}+\frac{\partial v}{\partial y}=0 \tag{2}$$

$$\begin{aligned}\left(u\frac{\partial u}{\partial x}+v\frac{\partial u}{\partial y}\right) &= u_\infty\frac{du_\infty}{dx}+\nu\left(1+\frac{1}{\beta}\right)\frac{\partial^2 u}{\partial y^2}\\ &-\frac{\sigma B_0^2}{\rho}(u-u_\infty)-\frac{\nu}{k'}(u-u_\infty)\\ &+g[\,\beta_T(T-T_M)+\beta_C(C-C_\infty)]\end{aligned} \tag{3}$$

$$\begin{aligned}\left(u\frac{\partial T}{\partial x}+v\frac{\partial T}{\partial y}\right) &= \alpha\frac{\partial^2 T}{\partial y^2}\\ &+\tau\left[D_B\frac{\partial C}{\partial y}\frac{\partial T}{\partial y}+\frac{D_T}{T_\infty}\left(\frac{\partial T}{\partial y}\right)^2\right]\\ &+\frac{D_m K_T}{C_x C_p}\frac{\partial^2 C}{\partial y^2}+\frac{\nu}{C_p}\left(1+\frac{1}{\beta}\right)\left(\frac{\partial u}{\partial y}\right)^2\\ &-\frac{1}{\rho C_p}\frac{\partial q}{\partial y},\end{aligned} \tag{4}$$

$$\begin{aligned}\left(u\frac{\partial C}{\partial x}+v\frac{\partial C}{\partial y}\right) &= D_B\frac{\partial^2 C}{\partial y^2}+\frac{D_T}{T_\infty}\frac{\partial^2 T}{\partial y^2}\\ &+\tfrac{D_m K_T}{T_m}\tfrac{\partial^2 T}{\partial y^2}-R^*(C-C_\infty).\end{aligned} \tag{5}$$

By using the Rosseland approximation of radiation [31], where, q can be written as:

$$q=-\frac{4\sigma^*}{3k^*}\frac{\partial T^4}{\partial y}. \tag{6}$$

Meanwhile, T^4 function as a linear equation for temperature that has been increased using the expansion of the series concerning T_∞ as: $T^4 \approx 4T_\infty^3 T - 3T_\infty^4$. Then,

$$\frac{\partial q}{\partial y}=-\frac{16\sigma^* T_\infty^3}{3k^*}\frac{\partial^2 T}{\partial y^2}. \tag{7}$$

In view of Eq. (6) and Eq. (7), Eq. (4) takes the form:

$$\begin{aligned}\left(u\frac{\partial T}{\partial x}+v\frac{\partial T}{\partial y}\right) &= \alpha\frac{\partial^2 T}{\partial y^2}\\ &+\tau\left[D_B\frac{\partial C}{\partial y}\frac{\partial T}{\partial y}+\frac{D_T}{T_\infty}\left(\frac{\partial T}{\partial y}\right)^2\right]\\ &+\frac{D_m K_T}{C_x C_p}\frac{\partial^2 C}{\partial y^2}+\frac{\nu}{C_p}\left(1+\frac{1}{\beta}\right)\left(\frac{\partial u}{\partial y}\right)^2\\ &-\frac{1}{\rho C_p}\frac{16\sigma^* T_\infty^3}{3k^*}\frac{\partial^2 T}{\partial y^2}.\end{aligned} \tag{8}$$

The boundary conditions that correspond to the current problem can be obtained as:

$$\begin{gathered}y=0\Rightarrow u(x)=u_w+\frac{\mu_f}{L}\left(1+\frac{1}{\beta}\right)\frac{\partial u}{\partial y},\\ T=T_M, C=C_w,\\ y\Rightarrow\infty\Rightarrow u\to u_\infty, T\to T_\infty, C\to C_\infty.\end{gathered} \tag{9}$$

$$k_t\left(\frac{\partial T}{\partial y}\right)_{y=0}=\rho[\lambda_M+c_s(T_M-T_0)]\,v(x,0) \tag{10}$$

Eq. (7) shows that the total heat delivered to the melting area consists of both the latent heat necessary for melting and the perceived heat required to raise the initial temperature of the solid to its melting point T_M. Similarity variables in view of Hayat et al. [30] are:

$$\begin{aligned}&\eta=y\sqrt{\frac{a}{\nu}}, \quad u=axF'(\eta), \quad v=-\sqrt{a\nu}F(\eta),\\ &u_\infty=bx, \quad \theta(\eta)=\frac{T-T_M}{T_\infty-T_M}, \phi(\eta)=\frac{C-C_\infty}{C_w-C_\infty}\end{aligned} \tag{11}$$

By applying similarity transformations in Eq. (11), Eq. (3), Eq. (5), and Eq. (8) are converted into the following ordinary differential equations (ODEs):

$$\begin{aligned}&\left(1+\frac{1}{\beta}\right)F'''+FF''-F'^2-(M+B^*)(\lambda^*-F')\\ &+\lambda^{*2}+(\lambda\theta+\delta\phi)=0,\end{aligned} \tag{12}$$

$$\begin{aligned}&\tfrac{1}{Pr}\left[1+\tfrac{4}{3}R_r\right]\theta''+F\theta'+Nt\theta'^2+Nb\theta'\phi'+\\ &Df\phi''+\left(1+\tfrac{1}{\beta}\right)EcF''^2=0,\end{aligned} \tag{13}$$

$$\phi''+ScF\phi'+\left(\frac{Nt}{Nb}+Sr\,Sc\right)\theta''-Sc\gamma\phi=0. \tag{14}$$

Finally, the resultant boundary conditions (5)-(6) are:

$$\begin{aligned}&F'(0)=1+Y\left(1+\frac{1}{\beta}\right)F''(0), \theta(0)=0,\\ &\phi(0)=1, F'(\infty)=\lambda^*,\ \theta(\infty)=1,\\ &\phi(\infty)=0,\ M_e\theta'(0)+\Pr F(0)=0,\end{aligned} \tag{15}$$

Without any dimensional specifications,

$$\begin{aligned}&\lambda=\frac{Gr_x}{Re_x^2}, \delta=\frac{Gc_x}{Re_x^2}, M=\frac{\sigma B_0^2}{\rho a}, \lambda^*=\frac{b}{a}, B^*=\frac{\nu}{ak'},\\ &Sc=\frac{\nu}{D_B}, \quad Pr=\frac{\nu}{\alpha}, \quad Nb=\frac{\tau D_B(C_w-C_\infty)}{\nu},\\ &Nt=\frac{\tau D_T(T_\infty-T_M)}{\nu T_\infty}, Gr_x=\frac{g\beta_T(T_\infty-T_M)x^3}{\nu^2},\\ &Gc_x=\frac{g\beta_c(C_w-C_\infty)x^3}{\nu^2}, \quad R_r=\frac{4\sigma^* T_\infty^3}{k_t K^*},\\ &Sr=\frac{D_m K_T}{T_m\nu}\frac{(T_\infty-T_M)}{(C_w-C_\infty)}, Df=\frac{D_m K_T}{\nu C_x C_p}\frac{(C_w-C_\infty)}{(T_\infty-T_M)},\\ &Ec=\frac{u_w^2}{C_p(T_\infty-T_M)}, \quad \gamma=\frac{R^*}{a}, \quad Y=\frac{\mu_f}{L}\sqrt{\frac{a}{\upsilon}}\end{aligned} \tag{16}$$

$M_e=\frac{C_p(T_\infty-T_M)}{\lambda_M+c_s(T_M-T_0)}$ which is a grouping of two Stefan numbers $\frac{c_f((T_\infty-T_M)}{\lambda_M}$ and $\frac{c_s((T_M-T_0)}{\lambda_1}$ for the liquid and solid states, consistently.

Physical variables that are important for understanding how fluid behaves at the surface include the local skin friction coefficient f_x, local Nusselt number Nu_x and local Sherwood number Sh_x, which are described as:

$$Cf_x=\frac{\tau_w}{\rho u_w{}^2}, Nu_x=\frac{xq_w}{k_t((T_\infty-T_M)}, Sh_x=\frac{xq_m}{D_B((C_w-C_\infty)}, \tag{17}$$

where, τ_w is shear stress through an extended plate, q_w is the heat flow from the surface, and q_m is the surface mass flux, which is drawn by:

$$\tau_w = \mu_B \left(1 + \frac{1}{\beta}\right)\left(\frac{\partial u}{\partial y}\right)_{y=0},$$
$$q_w = -k_t \left(\frac{\partial T}{\partial y}\right)_{y=0}, \quad (18)$$
$$q_m = -D_B \left(\frac{\partial C}{\partial y}\right)_{y=0},$$

Substituting equation:

$$C_f \sqrt{Re_x} = \left(1 + \frac{1}{\beta}\right) F''(0),$$
$$\frac{Nu_x}{\sqrt{Re_x}} = -\theta'(0),$$
$$\frac{Sh_x}{\sqrt{Re_x}} = -\phi'(0),$$

where, the local Reynolds number is $Re_x = \frac{xu_w}{\nu}$.

3. NUMERICAL TECHNIQUE

In 1971, Keller [32] used a numerical method to solve a boundary value problem in 1971. After a decade, Jones [33] employed this technique for numerical simulation in a boundary value problem. For the last three decades, researchers have used this technique for the numerical simulation of boundary-layer flow problems because it is very effective in producing accurate numerical results up to second-order convergence. In this study, a numerical solution was obtained using the Keller–Box method. In this scheme, first we convert higher-order ODEs into first-order ODEs, then write a difference equation using central differences, linearize these equations via the Newton method, write them in matrix form, and finally solve the matrices via the block-diagonal method. In addition, this method is straightforward to program, very user-friendly, and converges more quickly to the second order. For detailed characterization, Rafique et al. [34] discussed this technique in detail.

4. RESULTS AND DISCUSSION

This study investigates the MHD stagnation point flow and heat transfer of CNF over a vertically stretched sheet, taking into account velocity slip, as well as the Soret and Dufour effects. Brownian motion and thermophoresis are also considered. The governing equations of CNF flow in Eq. (12) to Eq. (14) are numerically solved, according to the boundary conditions in Eq. (15), to examine the flow and heat transfer properties. The research investigates how various controlling factors influence the velocity, temperature, and concentration profiles within the boundary layer region. The outcomes of different flow properties are analyzed and illustrated with graphs. Table 1 presents a comparison of our results for F" (0) those gotten by Mabood and Mabood and Mastro Berardino [35], Hayat et al. [36]. Table 2 shows a comparison of our results for F" (0) with those specified by Hayat et al. [37] and Ishak et al. [38] for various values of λ*. They found that the current results are both dependable and accurate. The present numerical calculations for $-\theta'(0)$ are compared to those published by Bachok et al. [39]. The findings in Tables 1-3 demonstrate a positive correlation.

Figure 2 illustrates how a fluid's velocity profile varies in response to a magnetic field M. It is noted that when M increased, the velocity and momentum boundary layer thicknesses decreased as well. It is due to the fluid's velocity decreasing because the magnetic field exerts a resistance to its motion. Figure 3 shows how the velocity profile is affected by the Casson parameter β. It demonstrates that the fluid velocity decreases as the value of β increases. This is because an increase in β enhances the fluid's resistance to flow, thereby reducing its velocity.

Table 1. Comparing the results of $F''(0)$ for different numbers of M at $M_e = Y = \lambda^* = 0, Pr = 1$

M	The Present Work	Mabood and Mastro Berardino [35]	Hayat et al. [36]
0	-1.00006	-1.000008	-1.00000
1	-1.41421	-1.4142135	-1.41421
5	-2.44948	-2.4494897	-2.44948
10	-3.31664	-3.3166247	-3.31662
50	-7.14148	-7.141484	-7.14142
100	-10.0496	-10.0497	-10.049875

Table 2. Comparing the results of $F''(0)$ for different numbers of λ^* with $Pr = 1$

λ^*	The Present Work	Hayat et al. [37]	Ishak et al. [38]
0.01	-0.998065	-0.99823	-0.9980
0.1	-0.969387	-0.96954	-0.9694
0.2	-0.918107	-0.91813	-0.9181
0.5	-0.667263	-0.66735	-0.6673
2	2.01741	2.01767	2.0175
3	4.72801	4.72964	4.7294

Table 3. Comparing the results of $-\theta'(0)$ for different numbers of M_e and Pr when $\lambda^* = 1$

Pr	M	The Present Work	Bachok et al. [39]
1	0	-0.7978740	-0.7978846
	1	-0.5060480	-0.5060545
	2	-0.3826380	-0.3826383
	3	-0.311960	-0.3119564
7	0	-2.11209	-2.1110042
	1	-1.34214	-1.3388943
	2	-1.01528	-1.0123657
	3	0.827734	-0.8253591

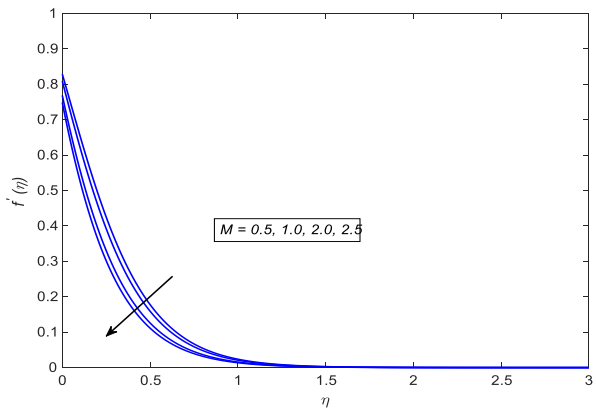

Figure 2. Velocity profile for the various values of M

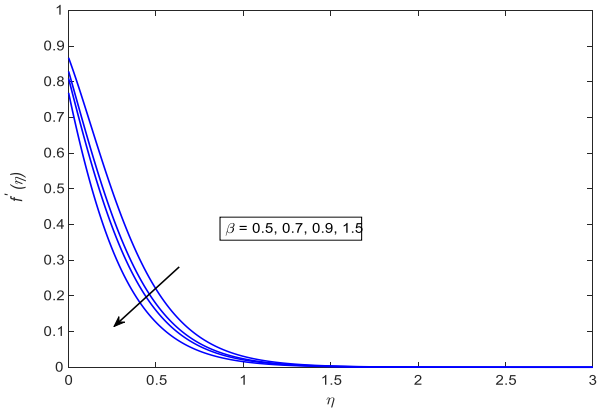

Figure 3. Velocity profile for various values of β

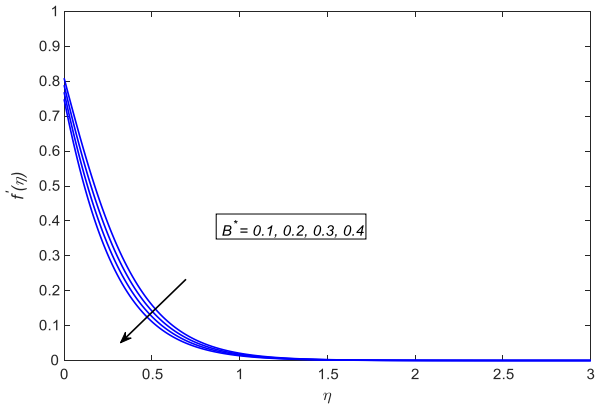

Figure 4. Velocity profile for the various values of B^*

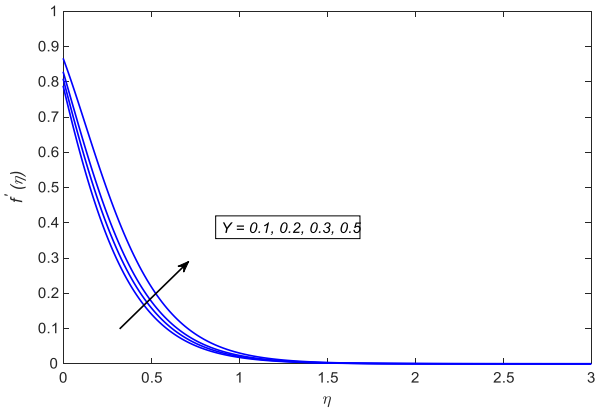

Figure 5. Velocity profile for different values of Y

Figure 4 shows the asterisk operator and end superscript on the velocity distribution. The velocity distribution decreases as the values of the porous parameter B^* rise. Physically, porosity typically acts as a sink of momentum, increasing resistance and decreasing velocity. Figure 5 illustrates how the velocity distribution is affected by the velocity slip parameter Y. This shows that when the value of the velocity slip parameter Y increases, the velocity profile increases. This effect occurs because the velocity slip condition typically reduces wall shear, allowing the fluid to move faster near the surface. Figure 6 indicates the impact of the Casson parameter β on the temperature profile. This figure shows that the temperature profile decreases as the value of β increases. This phenomenon can be attributed to reduced frictional resistance at the boundary, resulting in lower heat generation within the fluid.

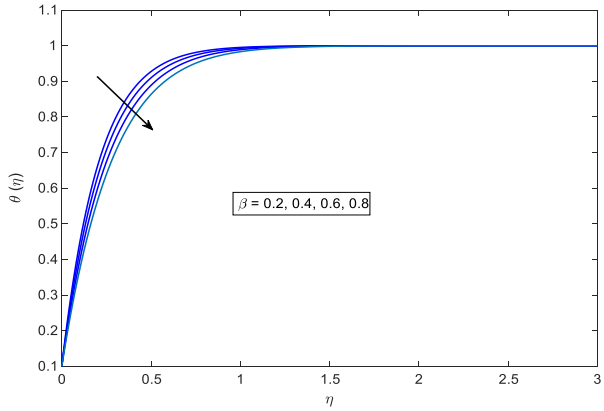

Figure 6. Temperature profile for various values of β

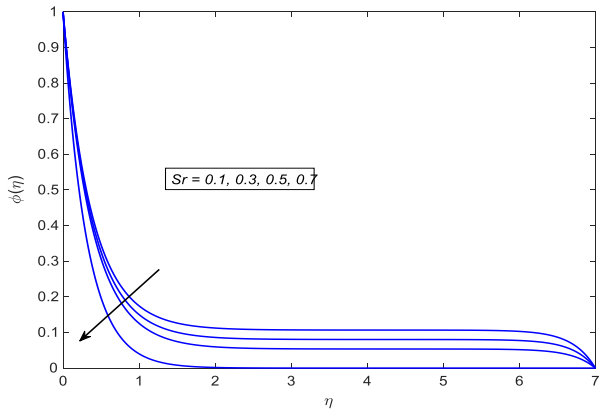

Figure 7. Concentration profile for various values of Sr

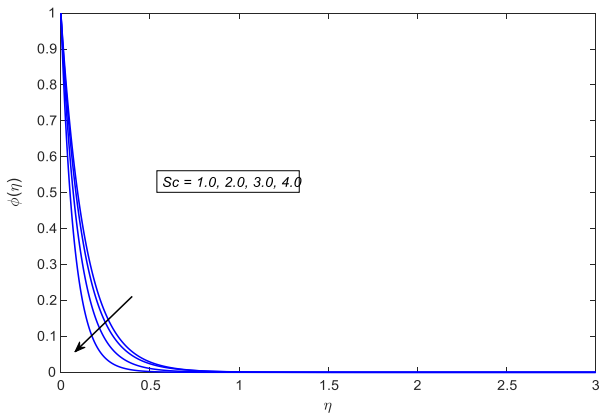

Figure 8. Concentration profile for various values of Sc

Figure 7 displays the impact of the Soret number Sr on the concentration profile. The concentration profile decreases as the Soret number increases. When the Soret number Sr increases, it indicates that particles migrate from high-temperature regions. Concentration profiles within the fluid are decreased as a result of this temperature dispersion.

Figure 8 shows how the concentration profile is affected by variations in Schmidt number. As the Schmidt number grows, the concentration profile decreases. The Schmidt number helps to understand the importance of momentum diffusivity and mass diffusivity within the fluid. Concentration profiles drop as the Schmidt number increases because mass diffusivity decreases with it.

Figure 9 displays the temperature profile for various Dufour number Df values. This variable specifies the relationship

between a fluid's mass and heat transport mechanisms. It shows that a rise in the Dufour number enhances the temperature profile, which increases the rate at which mass diffusion proceeds. When heat is transferred from a high-concentration to a low-concentration region, the temperature profile increases.

Figure 10 shows how the concentration profile is affected by the chemical reaction factor γ. The concentration profile reduces as the chemical reaction parameter γ rises. Figure 11 illustrates how the temperature profile is affected by the thermophoresis factor Nt. Heat-producing particles move away from the hotter area to the cooler area. The fluid's temperature changes as a result. As a result, the thermophoresis factor Nt increases, and the temperature profile also rises.

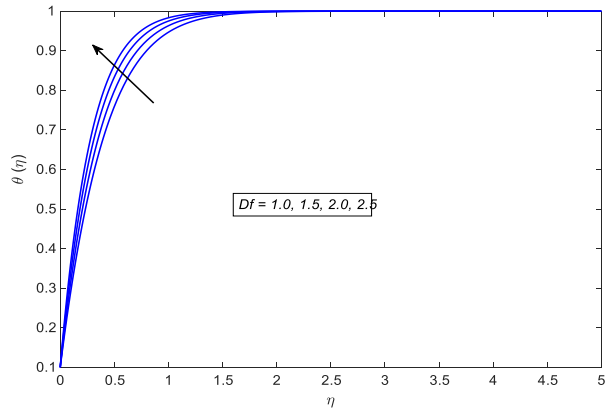

Figure 9. Temperature profile for various values of *Df*

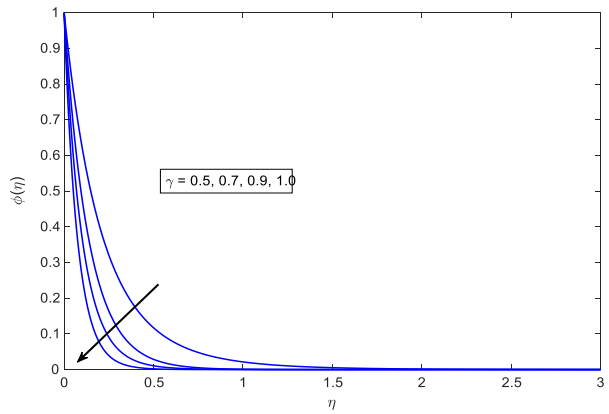

Figure 10. Concentration profile for various values of γ

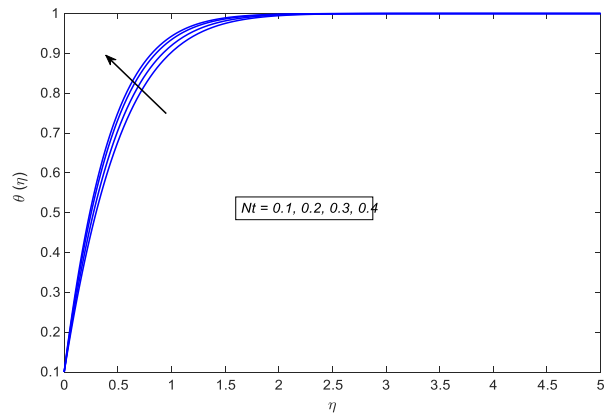

Figure 11. Temperature profile for various values of Nt

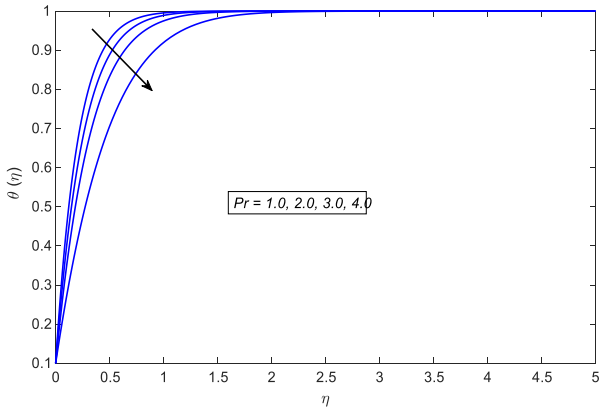

Figure 12. Temperature profile for various values of *Pr*

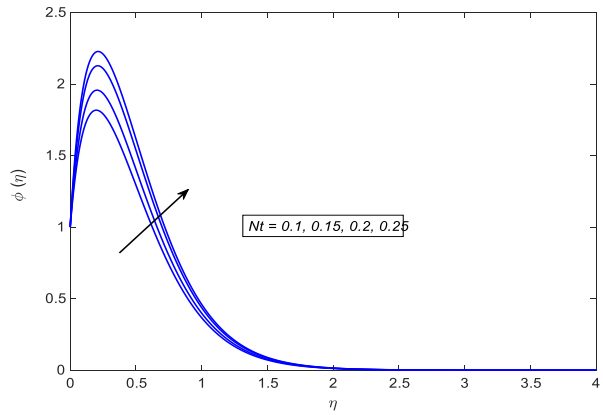

Figure 13. Concentration profile for various values of *Nt*

Figure 12 represents the behaviour of the temperature profile for various values of Prandtl number (*Pr*). It is observed that when the value of the *Pr* rises, the temperature profile decreases. Physically, the *Pr* is the ratio of momentum diffusivity to thermal diffusivity. An increase in *Pr* signifies a relative decrease in thermal diffusivity, which inhibits heat penetration and leads to a thinner thermal boundary layer and a decrease in the temperature profile within the boundary layer.

Figure 13 shows how the concentration profile is affected by the thermophoresis factor Nt. It has been shown that the concentration profile and the thermal boundary layer thickness both increase as the value of Nt. According to this result, a more concentrated profile within the fluid and a thicker concentration boundary layer are caused by larger Nt values.

5. CONCLUSIONS

This study investigates MHD stagnation-point flow and heat transfer of a CNF over a vertically stretched sheet, by incorporating velocity slip and the Soret and Dufour effects. Moreover, thermal radiation and chemical reactions are accounted for. In addition, Brownian motion and thermophoresis impacts are discussed graphically. For numerical results, the Keller–Box method is employed, which gives fast convergence up to second order in less time. Furthermore, the influence of porosity and slip effects on the velocity profile is presented via graphs. These are the main conclusions of this research:

- The velocity distribution increases with the growth of the slip parameter.

- The temperature profile decreases as the Casson parameter increases.
- The concentration profile decreases as the Soret effect increases.
- The velocity profile decreases with increasing porosity.
- The temperature profile increases as the Dufour effect parameter increases.

In the future, this research can be extended numerically to different geometries, including disks, cylinders, cones, and spheres. This investigation plays a key role in engineering and industry.

ACKNOWLEDGEMENT

The authors extend their appreciation to the Arab Open University for funding this work.

REFERENCES

[1] Tauviqirrahman, M., Jamari, J., Susilowati, S., Pujiastuti, C., Setiyana, B., Pasaribu, A.H., Ammarullah, M.I. (2022). Performance comparison of Newtonian and non-Newtonian fluid on a heterogeneous slip/No-slip journal bearing system based on CFD-FSI method. Fluids, 7(7): 225. https://doi.org/10.3390/fluids7070225

[2] Ionescu, C.M., Birs, I.R., Copot, D., Muresan, C.I., Caponetto, R. (2020). Mathematical modelling with experimental validation of viscoelastic properties in non-Newtonian fluids. Philosophical Transactions of the Royal Society A, 378(2172): 20190284. https://doi.org/10.1098/rsta.2019.0284

[3] Ullah, I., Nisar, K.S., Shafie, S., Khan, I., Qasim, M., Khan, A. (2019). Unsteady free convection flow of Casson nanofluid over a nonlinear stretching sheet. IEEE Access, 7: 93076-93087. https://doi.org/10.1109/ACCESS.2019.2920243

[4] Lee, C., Nadeem, S. (2017). Numerical study of non-Newtonian fluid flow over an exponentially stretching surface: An optimal HAM validation. Journal of the Brazilian Society of Mechanical Sciences and Engineering, 39(5): 1589-1596. https://doi.org/10.1007/s40430-016-0687-3

[5] Elgazery, N.S., Elelamy, A.F. (2020). Multiple solutions for non-Newtonian nanofluid flow over a stretching sheet with nonlinear thermal radiation: Application in transdermal drug delivery. Pramana, 94(1): 68. https://doi.org/10.1007/s12043-020-1925-x

[6] Lone, S.A., Anwar, S., Saeed, A., Bognár, G. (2023). A stratified flow of a non-Newtonian Casson fluid comprising microorganisms on a stretching sheet with activation energy. Scientific Reports, 13(1): 11240. https://doi.org/10.1038/s41598-023-38260-0

[7] Prameela, M., Gangadhar, K., Reddy, G.J. (2022). MHD free convective non-Newtonian Casson fluid flow over an oscillating vertical plate. Partial Differential Equations in Applied Mathematics, 5: 100366. https://doi.org/10.1016/j.padiff.2022.100366

[8] Ali, F.M., Khamat, A.N.A., Junoh, M.M. (2021). Dual solutions in mixed convection stagnation-point flow over a vertical stretching sheet with external magnetic field and radiation effect. Journal of Advanced Research in Fluid Mechanics and Thermal Sciences, 80(2): 22-32. https://doi.org/10.37934/arfmts.80.2.2232

[9] Khan, S.A., Ali, B., Eze, C., Lau, K.T., Ali, L., Chen, J., Zhao, J. (2021). Magnetic dipole and thermal radiation impacts on stagnation point flow of micropolar based nanofluids over a vertically stretching sheet: Finite element approach. Processes, 9(7): 1089. https://doi.org/10.3390/pr9071089

[10] Ghasemi, S.E., Hatami, M. (2021). Solar radiation effects on MHD stagnation point flow and heat transfer of a nanofluid over a stretching sheet. Case Studies in Thermal Engineering, 25: 100898. https://doi.org/10.1016/j.csite.2021.100898

[11] Yasin, S.H.M., Mohamed, M.K.A., Ismail, Z., Salleh, M.Z. (2020). Mathematical solution on MHD stagnation point flow of ferrofluid. In Defect and Diffusion Forum, pp. 38-54. https://doi.org/10.4028/www.scientific.net/DDF.399.38

[12] Alhamaly, A.S., Khan, M., Shuja, S.Z., Yilbas, B.S., Al-Qahtani, H. (2021). Axisymmetric stagnation point flow on linearly stretching surfaces and heat transfer: Nanofluid with variable physical properties. Case Studies in Thermal Engineering, 24: 100839. https://doi.org/10.1016/j.csite.2021.100839

[13] Alrehili, M. (2024). Nanofluid dissipative stagnation point flow of Casson type over a stretched sheet influenced by a variable surface heat flux and magnetic field. Results in Physics, 58: 107535. https://doi.org/10.1016/j.rinp.2024.107535

[14] Choi, S.U. (1995). Enhancing thermal conductivity of fluids with nanoparticles. In Proceedings of the ASME 1995 International Mechanical Engineering Congress and Exposition: Developments and Applications of Non-Newtonian Flows, San Francisco, USA, pp. 99-105. https://doi.org/10.1115/IMECE1995-0926

[15] Buongiorno, J. (2006). Convective transport in nanofluids. Journal of Heat Transfer, 128(3): 240-250. https://doi.org/10.1115/1.2150834

[16] Aljaloud, A.S., Manai, L., Tlili, I. (2024). Flow of couple stress nanofluid due to stretching surface with applications of induced magnetic field and variable thermal conductivity. Case Studies in Thermal Engineering, 57: 104356. https://doi.org/10.1016/j.csite.2024.104356

[17] Hosseinzadeh, K., Mardani, M.R., Paikar, M., Hasibi, A., et al. (2023). Investigation of second grade viscoelastic non-Newtonian nanofluid flow on the curve stretching surface in presence of MHD. Results in Engineering, 17: 100838. https://doi.org/10.1016/j.rineng.2022.100838

[18] Sedki, A.M. (2022). Effect of thermal radiation and chemical reaction on MHD mixed convective heat and mass transfer in nanofluid flow due to nonlinear stretching surface through porous medium. Results in Materials, 16: 100334. https://doi.org/10.1016/j.rinma.2022.100334

[19] Rafique, K., Nasim, A., Alshehery, S., Younas, B., Khan, I., Khan, M.S. (2025). Thermal radiation and stability aanalysis in dual solutions of Al_2O_3-Cu/H_2O hybrid nanofluid flow over a stretching/shrinking surface with Arrhenius kinetic energy. Journal of Radiation Research and Applied Sciences, 18(2): 101510. https://doi.org/10.1016/j.jrras.2025.101510

[20] Rafique, K., Kanwal, S., Niazai, S., Alqahtani, A.A., Khan, I. (2025). Significance of thermal radiation in stability analysis and triple solutions for magnetized

micropolar Buongiorno's nanofluid model. Journal of Radiation Research and Applied Sciences, 18(1): 101316. https://doi.org/10.1016/j.jrras.2025.101316
[21] Rafique, K., Khan, I., Bakouri, M. (2025). Newtonian heating effects on Casson nanofluid flow at lower stagnation point of a solid sphere. ZAMM-Journal of Applied Mathematics and Mechanics/Zeitschrift für Angewandte Mathematik und Mechanik, 105(1): e202300873. https://doi.org/10.1002/zamm.202300873
[22] Hussain, A., Afzal, S., Rizwana, R., Malik, M.Y. (2020). MHD stagnation point flow of a Casson fluid with variable viscosity flowing past an extending/shrinking sheet with slip effects. Physica A: Statistical Mechanics and Its Applications, 553: 124080. https://doi.org/10.1016/j.physa.2019.124080
[23] Raza, J. (2019). Thermal radiation and slip effects on magnetohydrodynamic (MHD) stagnation point flow of Casson fluid over a convective stretching sheet. Propulsion and Power Research, 8(2): 138-146. https://doi.org/10.1016/j.jppr.2019.01.004
[24] Narender, G., Govardhan, K., Sarma, G.S. (2020). Magnetohydrodynamic stagnation point on a Casson nanofluid flow over a radially stretching sheet. Beilstein Journal of Nanotechnology, 11: 1303-1315. https://doi.org/10.3762/bjnano.11.114
[25] Verma, K., Basfor, S., Sharma, B.R. (2020). Analysis of radiation, chemical reaction, Soret and Dufour effects near stagnation point on MHD flow through a stretching sheet. Advances in Mathematics: Scientific Journal, 10: 855-868. https://doi.org/10.37418/amsj.10.2.15
[26] Duguma, K.A., Makinde, O.D., Enyadene, L.G. (2023). Dual solutions and stability analysis of Cu-H_2O-Casson nanofluid convection past a heated stretching/shrinking slippery sheet in a porous medium. Computational and Mathematical Methods, 2023(1): 6671523. https://doi.org/10.1155/2023/6671523
[27] Mustafa, M., Hayat, T., Ioan, P., Hendi, A. (2012). Stagnation-point flow and heat transfer of a Casson fluid towards a stretching sheet. Zeitschrift für Naturforschung A, 67(1-2): 70-76. https://doi.org/10.5560/ZNA.2011-0057
[28] Kumar, R.K., Varma, S.V.K. (2019). Stagnation point flow of thermally radiative and dissipative MHD nanofluid over a stretching sheet filled with porous medium and suction. Songklanakarin Journal of Science and Technology, 41(1): 123-135. https://doi.org/10.14456/sjst-psu.2019.15
[29] Zulkifli, S.N.B., Sarif, N.M., Salleh, M.Z., Azmi, E.F. (2019). MHD stagnation point flow of micropolar nanofluid with Soret and Dufour effects. Journal of Physics: Conference Series, 1366: 012015. https://doi.org/10.1088/1742-6596/1366/1/012015
[30] Hayat, T., Kiran, A., Imtiaz, M., Alsaedi, A. (2017). Melting heat and thermal radiation effects in stretched flow of an Oldroyd-B fluid. Applied Mathematics and Mechanics, 38(7): 957-968. https://doi.org/10.1007/s10483-017-2218-6
[31] Viskanta, R., Grosh, R.J. (1962). Boundary layer in thermal radiation absorbing and emitting media. International Journal of Heat and Mass Transfer, 5(9): 795-806. https://doi.org/10.1016/0017-9310(62)90180-1
[32] Keller, H.B. (1971). A new difference scheme for parabolic problems. In Numerical Solution of Partial Differential Equations–II, pp. 327-350. https://doi.org/10.1016/B978-0-12-358502-8.50014-1
[33] Jones, E. (1981). An asymptotic outer solution applied to the Keller box method. Journal of Computational Physics, 40(2): 411-429. https://doi.org/10.1016/0021-9991(81)90219-9
[34] Rafique, K., Alqahtani, A.M., Ahmad, S., Aslam, S., Khan, I., Singh, A. (2024). Numerical simulations of Williamson fluid containing hybrid nanoparticles via Keller box technique. Discover Applied Sciences, 6(3): 80. https://doi.org/10.1007/s42452-024-05729-0
[35] Mabood, F., Mastro Berardino, A. (2015). Melting heat transfer on MHD convective flow of a nanofluid over a stretching sheet with viscous dissipation and second order slip. Journal of the Taiwan Institute of Chemical Engineers, 57: 62-68. https://doi.org/10.1016/j.jtice.2015.05.020
[36] Hayat, T., Hussain, Q., Javed, T. (2009). The modified decomposition method and Padé approximants for the MHD flow over a non-linear stretching sheet. Nonlinear Analysis: Real World Applications, 10(2): 966-973. https://doi.org/10.1016/j.nonrwa.2007.11.020
[37] Hayat, T., Mustafa, M., Shehzad, S.A., Obaidat, S. (2012). Melting heat transfer in the stagnation-point flow of an upper-convected Maxwell (UCM) fluid past a stretching sheet. International Journal for Numerical Methods in Fluids, 68(2): 233-243. https://doi.org/10.1002/fld.2503
[38] Ishak, A., Nazar, R., Arifin, N.M., Pop, I. (2007). Mixed convection of the stagnation-point flow towards a stretching vertical permeable sheet. Malaysian Journal of Mathematical Sciences, 1(2): 217-226.
[39] Bachok, N., Ishak, A., Pop, I. (2010). Melting heat transfer in boundary layer stagnation-point flow towards a stretching/shrinking sheet. Physics Letters A, 374(40): 4075-4079. https://doi.org/10.1016/j.physleta.2010.08.032

NOMENCLATURE

Latin symbol

B_0	Magnetic field strength (T)
C	Nanoparticle concentration
C_p	Specific heat capacity ($J \cdot kg^{-1} \cdot K^{-1}$)
CNF	Casson nanofluid
D_B	Brownian diffusion coefficient ($m^2 \cdot s^{-1}$)
D_m	Molecular diffusivity ($m^2 \cdot s^{-1}$)
D_T	Thermophoretic diffusion coefficient ($m^2 \cdot s^{-1} \cdot K^{-1}$)
F	Dimensionless stream function
k_t	Thermal conductivity ($W \cdot m^{-1} \cdot K^{-1}$)
L	Characteristic length (m)
MHD	Magnetohydrodynamics
μ_B	Plastic dynamic viscosity (Pa·s)
μ_f	Effective viscosity (Pa·s)
q	Heat flux ($W \cdot m^{-2}$)
ρ_f	Fluid density ($kg \cdot m^{-3}$)
T	Temperature (K)
u	Velocity in x-direction ($m \cdot s^{-1}$)
v	Velocity in y-direction ($m \cdot s^{-1}$)
θ	Dimensionless temperature
ϕ	Dimensionless concentration

Greek symbols

α	Thermal diffusivity ($m^2 \cdot s^{-1}$)
β	Casson fluid parameter
β_C	Concentration expansion coefficient
β_T	Thermal expansion coefficient (1/K)
δ	Solutal buoyancy parameter
γ	Chemical reaction parameter
λ	Thermal buoyancy parameter
M	Magnetic parameter
Nb	Brownian motion parameter
Nt	Thermophoresis parameter
P_y	Yield stress of Casson fluid (Pa)
π	Strain-rate invariant
π_c	Critical strain-rate threshold
Pr	Prandtl number
R_r	Radiation parameter
Sc	Schmidt number
Sr	Soret number
τ	Stress tensor (Pa)
Y	Velocity slip parameter
Df	Dufour number
Ec	Eckert number

Subscripts

0	Initial value
c	Critical value
f	Fluid property
M	Melting state / melting temperature
m	Mass flux / mass transfer
w	Wall or surface value
x	Local value in x-direction
∞	Ambient / free-stream condition
$y = 0$	At the surface
$y \to \infty$	Far from the surface